Journal of Power Sources 230 (2013) 230–235

Contents lists available at SciVerse ScienceDirect

Journal of Power Sources

journal homepage: www.elsevier.com/locate/jpowsour

Short communication

Influence of the configuration in planar interdigitated electrochemical micro-capacitors

David Pech [a,b,*], Magali Brunet [a,b], Ty Mai Dinh [a,b], Kevin Armstrong [c], Julie Gaudet [c], Daniel Guay [c]

[a] CNRS, LAAS, 7 avenue du colonel Roche, F-31400 Toulouse, France
[b] Univ de Toulouse, LAAS, F-31400 Toulouse, France
[c] INRS-Énergie, Matériaux, Télécommunications, 1650 boulevard Lionel Boulet, J3X 1S2 Varennes, Québec, Canada

HIGHLIGHTS

- The geometric configuration plays a key-role on the performances of μ-SCs.
- The reduction of the interspace enhances the specific energy and power.
- A high resolution μ-SC with interspace as low as 5 μm has been realized.
- The RuO_2 based μ-SC was able to cycle up to 100 V s^{-1}.

ARTICLE INFO

Article history:
Received 18 October 2012
Accepted 9 December 2012
Available online 23 December 2012

Keywords:
Micro-supercapacitors
RuO_2
Interdigitated electrode
ESR

ABSTRACT

We have investigated the influence of the geometric configuration of planar interdigitated micro-supercapacitors on their specific energy and specific power. The theoretical values of the Equivalent Series Resistance (ESR) were deduced from an analytical expression of the cell constant K, and compared with experimental Electrochemical Impedance Spectroscopy (EIS) measurements performed on gold current collectors with different interdigitated patterns (varying the interspace, width, length and number of interdigitated fingers). It is shown that the configuration plays a key-role on the electrochemical performances of the device, and that the specific power is enhanced by a reduction of the interspace.

Based on these results, we have realized hydrous RuO_2-based thin films electrochemical capacitors integrated on silicon with an optimized configuration, using conventional photolithography techniques and electrodeposition from an aqueous chloride solution. The micro-supercapacitor is characterized by a cell capacitance of 0.2 mF cm^{-2} per footprint area, and was able to cycle at a scan rate of 100 V s^{-1}.

1. Introduction

The reduction in size and power consumption of electronic circuits, sensors and actuators, has enabled the development of embedded micro-systems with greater autonomy of energy. Accordingly, harvesting micro-devices that are able to extract energy from various ambient environmental sources (thermal, mechanical, solar energy) have received an increasing research interest, in the aim of obtaining autonomous self-powered systems [1]. The source of energy is not however continuously available in the environment and an intermediate rechargeable energy storage component as close as possible to the harvesting micro-device is essential to ensure the energy autonomy of the whole system. The harvested energy may be stored in micro-batteries (Li or Li-ions) [2], but their finite life-time may be problematic when they have to be embedded in systems with limited accessibility, such as structure-embedded micro-sensors where no maintenance or replacement is possible. Micro-batteries are moreover inefficient to supply loading applications requiring high amount of power.

The high power and extended lifetime of electrochemical capacitors, miniaturized to a microscopic scale, could satisfy a variety of micro-power demands and complement or replace micro-batteries in electrical energy storage and harvesting applications when high power delivery or uptake pulses are required in very short times. The integration of low-profile supercapacitors on a chip has thus been an emerging and increasing field of research over the last decade. Two categories of supercapacitors are

* Corresponding author. CNRS, LAAS, 7 avenue du colonel Roche, F-31400 Toulouse, France. Tel.: +33 5 61 33 68 37; fax: +33 5 61 33 62 08.
E-mail address: dpech@laas.fr (D. Pech).

0378-7753/$ – see front matter © 2012 Elsevier B.V. All rights reserved.
http://dx.doi.org/10.1016/j.jpowsour.2012.12.039

distinguished: electric double layer capacitors (EDLCs) based on carbon (activated carbon, nanostructured carbon) and pseudo-capacitors based on metal oxides such as RuO_2, MnO_2 or conductive polymers such as polypyrrole.

The first micro-supercapacitors (μ-SCs) were inspired from the technologies developed for micro-batteries, using a solid-state RuO_2/LiPON electrode/electrolyte in a stacked configuration [3–5]. Several other solid electrolytes were then experimented with the same configuration [6–8]. However, the stack configuration is limited to solid or gel-type electrolytes, which generally leads to a loss of power. Furthermore, in terms of integration, it can be very challenging as it requires numerous processing steps to pattern the different layers: current collectors, active material, electrolyte and to establish electrical connections at the end. μ-SCs based on pseudo-capacitive materials [9–13] and carbon-based electric double-layer micro-capacitors [14–18] have been afterward realized on planar configuration, where electrodes of various shapes are fabricated on a same plane and electronically isolated by a physical separation. This configuration, mostly interdigitated, has indeed the advantages of easy fabrication with limited number of technological steps, suitability with all types of electrolytes (including liquid), and an easy adjustment of the patterns, which can decrease the internal impedance by minimizing the distance between adjacent electrodes [15,19].

An electrical energy storage micro-device has a limited surface area available in the electronic circuit. Following the approach taken for ion transport in 3D-microbattery [20], it is important to optimize the geometry of the current collectors for a given electrode material and to consider the performances of the μ-SC (capacitance, energy and power) normalized to its footprint area on the chip.

In the present work, we have investigated the influence of the geometric parameters (interspace *i*, width *w*, length *L* and number of fingers *N*) of planar interdigitated μ-SCs on their electrochemical performances (specific energy and power per footprint area). Theoretical values were compared with experimental electrochemical impedance spectroscopy (EIS) measurements performed on different patterns. Then, the optimal configuration was used for the realization of an interdigitated μ-SC with RuO_2 as the active material. Hydrous forms of ruthenium dioxide $RuO_x \cdot nH_2O$ (denoted RuO_2 thereafter) currently represent the state of the art in pseudo-capacitive materials, with high capacitance (up to 1575 F g^{-1}), high electric conductivity (300 S cm^{-1}) and excellent cycle life (>10^5 cycles). Its high cost has limited its development for large-size supercapacitors, but the use of this material becomes relevant and promising for μ-SCs using very little amount of active material [21].

2. Experimental

Hydrous RuO_2 based μ-SCs were elaborated with different interdigitated patterns as shown in Fig. 1. The interspace *i* was varied from 5 to 100 μm, the width *w* from 50 to 200 μm, the length *L* from 100 to 1000 μm, and the number of interdigitated fingers *N* from 2 to 60. The width of the component (which is the sum of the width of both pads, the interspace *i* and the length *L* of the fingers) was set to 1700 μm. The micro-devices were realized as follows: a 500 nm SiO_2 was first thermally grown at 1100 °C on a silicon wafer. Current collectors were then deposited using the evaporation of a 100 nm Ti/800 nm Au layer, annealed at 250 °C for 20 min, and patterned with a conventional lift-off process. The current collectors and the pads were protected by an insulating layer (40 nm Si_3N_4/1 μm SiO_2) via a plasma enhanced chemical vapor deposition (PECVD). The interdigitated gold fingers where the active material will be subsequently deposited were then selectively opened via a second photolithography step followed by the

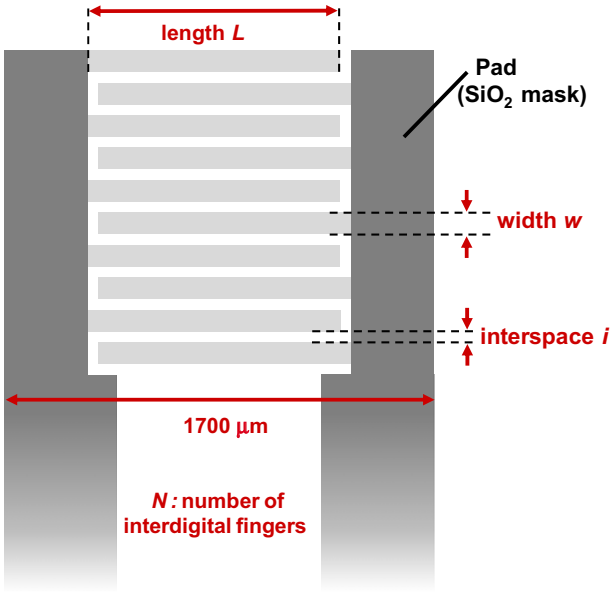

Fig. 1. Schematic drawing of the interdigital micro-device.

etching of the masking Si_3N_4/SiO_2 layer in a buffered HF. The current collectors were finally cleaned in a sulfochromic acid solution.

Electrodeposition of hydrous ruthenium oxide onto gold current collectors was carried out from an aqueous chloride solution composed of 10 mM $RuCl_3 \cdot xH_2O$ in 10^{-1} M KCl/10^{-2} M HCl, and adjusted to pH 2 with a KOH aqueous solution. Cyclic voltammetry (CV) between −300 and +950 mV vs. Ag/AgCl at 50 mV s^{-1}, and performed at 50 °C for 100 cycles under stirring conditions, was used to induce the growth of the RuO_2 deposits [22].

Electrochemical characterization of the electrodes and the micro-devices were performed in deaerated 0.5 M H_2SO_4 electrolyte using a SP-240 potentiostat from BioLogic equipped with a linear scan generator for high scan rates. EIS measurements were carried out at open circuit potential and frequencies ranging from 1 MHz to 10 mHz. The resistivity of the deposited gold, ρ_{Au}, was 2.2 μΩ cm and the electrolyte (0.5 M H_2SO_4) resistivity, ρ_e, was 5.1 Ω cm at 19.7 °C. Scanning Electron Microscopy (SEM) was performed using a Hitachi S-4800 field-emission electron microscope.

3. Results and discussions

3.1. Theoretical determination of the ESR of planar interdigitated electrodes

An electrochemical capacitor may be represented by an ideal capacitor with an "equivalent series resistance" (ESR) increased by an "equivalent distributed resistance" (EDR) related to the distributed resistance/capacitance of the porous electrode, as defined by R. Kötz [23]. The main contributions of the ESR are the current collector resistance, R_{cc}, and the electrolyte resistance, R_e, which both depend on the configuration of the micro-cell, while the EDR depends on the properties of the active material (porosity, thickness, nanostructuration…). Therefore, the specific power will predominantly depend on the highest resistive contribution between the ESR and the EDR. In order to focus on the influence of the geometric configuration on the performances of the cell, it is hypothesized in the following that the EDR is negligible compared to the ESR. This particular case is applicable to low-EDR active materials having a fully accessible surface area such as onion-like

carbon [15], graphene [24,25] and thin films, for which the influence of the configuration of the micro-device is prominent.

The resistance of the current collectors, R_{cc}, for the different geometries was estimated from Ohm's law using a Comsol simulation, and further validated experimentally with Kelvin probes using an Agilent 4294A impedance analyzer. As it will be shown later on (see Fig. 2), R_{cc} varies only slightly with i, w, L and N.

The theoretical values of the electrolyte resistance of the micro-devices, R_e, (which is given by $R_e = \mathrm{K} \times \rho_e$) have been deduced from the analytical expression of the cell constant, K, of planar interdigitated electrodes developed by W. Olthuis et al. [26], according to the following equation:

$$\mathrm{K} = \frac{1}{(N-1)\times L} \times \frac{2 \times K(k)}{K\left(\sqrt{(1-k^2)}\right)} \quad (1)$$

with $K(k)$ the complete elliptic integral of the first kind and

$$k = \frac{i}{i+w} \quad \text{for } N = 2 \quad (2)$$

$$k = \cos\left(\frac{\pi}{2}\frac{w}{i+w}\right) \quad \text{for } N > 2 \quad (3)$$

In Fig. 2, the value of ESR, which is given by the sum of R_{cc} and R_e, has been calculated for a series of interdigitated electrodes, starting from a unique configuration set to $i = 5$ μm, $w = 100$ μm, $L = 1000$ μm and $N = 10$, and allowing one single parameter to vary in each case. This was done using previously calculated values of R_{cc} and Eq. (1) in a Matlab environment to compute the value of K (and therefore R_e). In all cases, the electrolyte was assumed to be 0.5 M H_2SO_4.

As shown in Fig. 2(a), a micro-scale reduction of the interspace i between adjacent fingers (with $w = 100$ μm, $L = 1000$ μm and $N = 10$) significantly reduces the contribution of the resistance of the electrolyte R_e and the resulting ESR. It is noteworthy that a decrease of the interspace i does not have any effect on the active area, A_a, of the micro-devices since $A_a = N \times w \times L = 1$ mm^2. Increasing the width w, the length L or the number of fingers N (Fig. 2(b)–(d), respectively) lead to an increase of the active area A_a, and therefore, as expected, to a decrease of R_e and ESR.

A series of interdigitated electrodes were prepared with various values of i, w, L and N to validate the proposed model. The ESR values of the interdigitated electrodes were determined from EIS measurements performed in 0.5 M H_2SO_4 electrolyte. The ESR values were taken at the intersection point on the real axis at high frequency. As shown in Fig. 2, all the experimentally measured ESR values (without any active material) are in close agreement with the theoretically determined values, except for the case of $i > 40$ μm, where the calculated ESR values slightly overestimate the experimentally determined values. This could be due to fringing effects [26]. In the following, we will focus on the study of interdigitated electrode with $i = 5$ μm, where the proposed model is validated by the experimental data. Also, focusing on a given electrode material and a given electrolyte, it is now important to

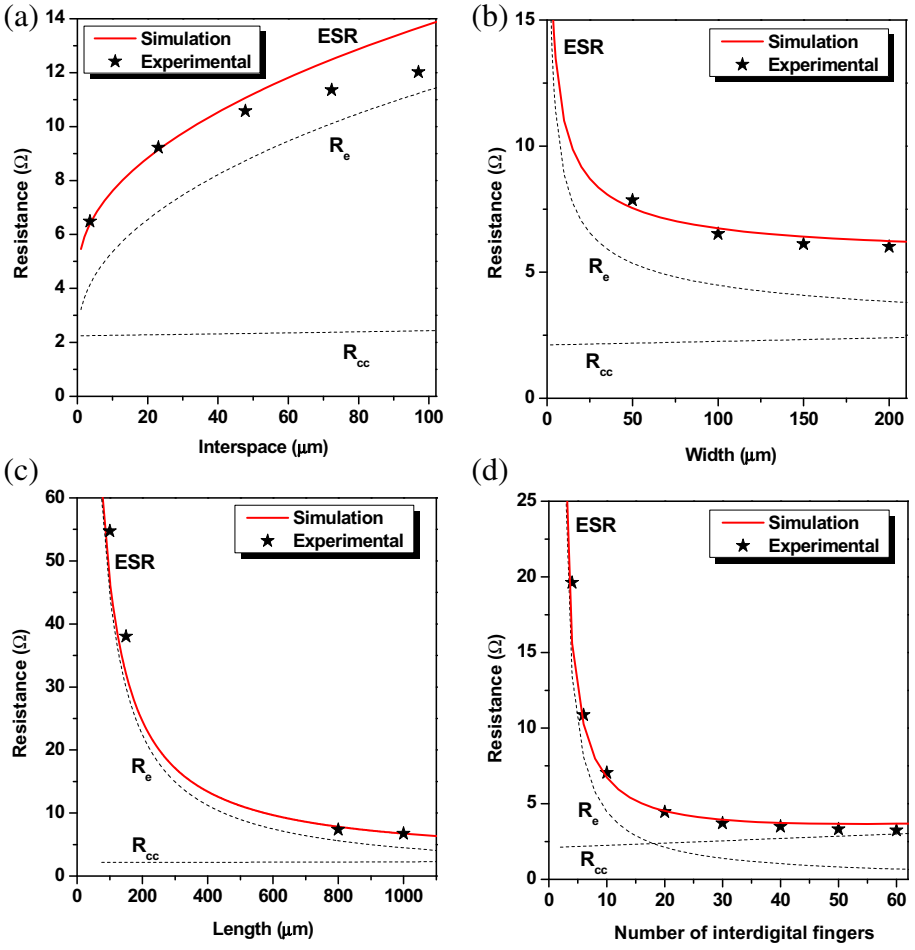

Fig. 2. Theoretical and Experimental evolution of R_e, R_{cc} and ESR as a function of (a) the interspace i, (b) the width w, (c) the length L, (d) the number of interdigital fingers N.

study how the interdigitated configuration will affect the maximum specific energy and power that can be drawn from the device.

3.2. Influence of the configuration on the specific energy and power

As seen before, it is important to normalize the properties of μ-SCs by the footprint aera, A_{fp}. The specific energy per footprint area, E_{fp} (in mJ cm^{-2}), can be determined by the following equation:

$$E_{fp} = \frac{C\Delta U^2}{2 \times A_{fp}} \quad (4)$$

with ΔU the potential range (in V).

As the absolute capacitance C (in F) is directly related to the active area, A_a, the maximum specific energy will be obtained by maximizing the ratio A_a/A_{fp}. This will be achieved by increasing the values of w and decreasing the values of i.

Concerning the maximum usable power per footprint area, P_{fp} (in mW cm^{-2}), it is calculated according to the following equation:

$$P_{fp} = \frac{\Delta U^2}{4 \times R \times A_{fp}} \quad (5)$$

with R = ESR + EDR, the total effective resistance. Neglecting the EDR (see below), Eq. (5) becomes:

$$P_{fp} = \frac{\Delta U^2}{4 \times (R_{cc} + R_e) \times A_{fp}} \quad (6)$$

Both R_{cc} and A_{fp} will increase with an augmentation of one of the geometric parameters of the interdigitated fingers (i, w, L or N). Also, as $R_e(i)$ is an increasing function, the best configuration for increasing $P_{fp}(i)$ will always be the one favoring the lowest interspace i. Finally, $R_e(w)$, $R_e(L)$ and $R_e(N)$ are all decreasing functions. Therefore, $P_{fp}(w)$, $P_{fp}(L)$and $P_{fp}(N)$ will have a maximum that will depend on both the geometry of the component and the properties of the current collectors (thickness, material).

Based on these results, we have realized interdigitated RuO_2 based μ-SCs with optimized configuration for enhanced performances.

3.3. Applications to RuO_2 based interdigitated micro-supercapacitors

3.3.1. Simulation of the optimized configuration

The above procedure was applied to determine the best configuration for the realization of interdigitated RuO_2-based μ-SCs with an electrode capacitance of 1.2 mF cm^{-2} (per active area) and negligible EDR (see below), according to the geometric specifications shown in Fig. 1 (footprint area $A_{fp} = 1700 \times N \times (w + i)$).

Fig. 3 shows the theoretical evolution of the specific energy E_{fp} and specific power P_{fp} per footprint area based on Eqs. (1), (4) and (6), and using a 1 V potential range. Just like before, a single geometric parameter was varied at a time, starting from an initial configuration set to $i = 5$ μm, $w = 100$ μm, $L = 1000$ μm and $N = 10$. The specific energy and specific power are both favored for the lowest interspace i (Fig. 3(a)) and highest length L (Fig. 3(c)). Increasing the width w increases the specific energy E_{fp}, but at the expanse of the specific power P_{fp} (Fig. 3(b)). Regarding the number

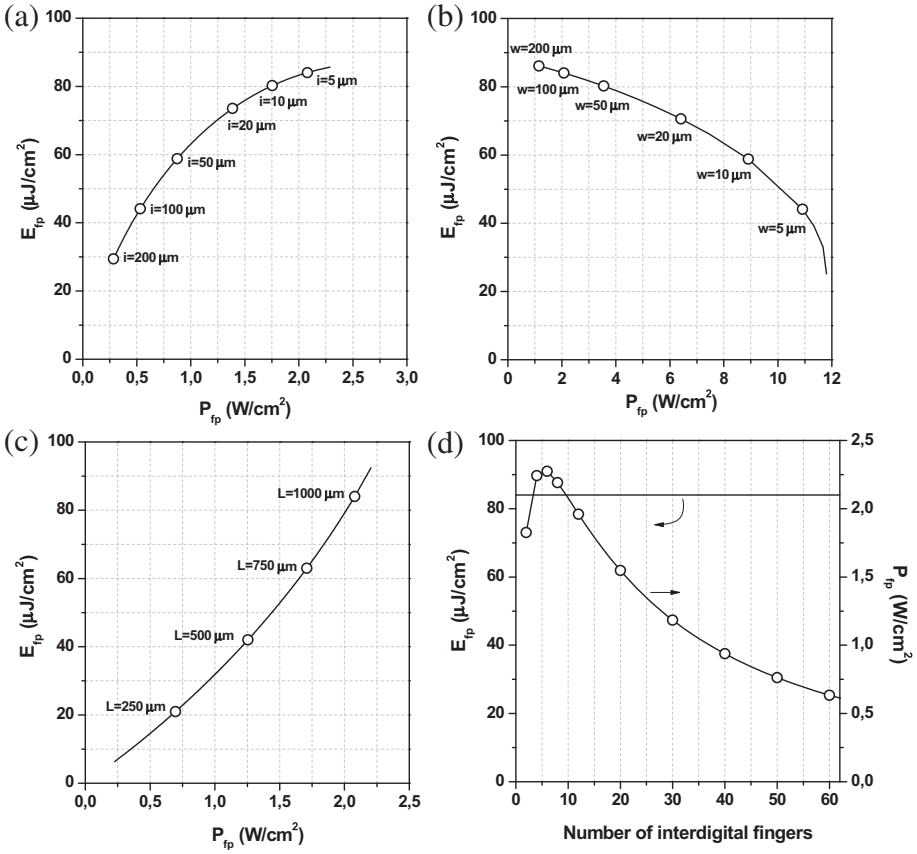

Fig. 3. Theoretical evolution of the specific energy E_{fp} and specific power P_{fp} per footprint area for a RuO_2 μ-SC of 1.2 mF cm^{-2} electrode capacitance as a function of (a) the interspace i, (b) the width w, (c) the length L, (d) the number of interdigital fingers N.

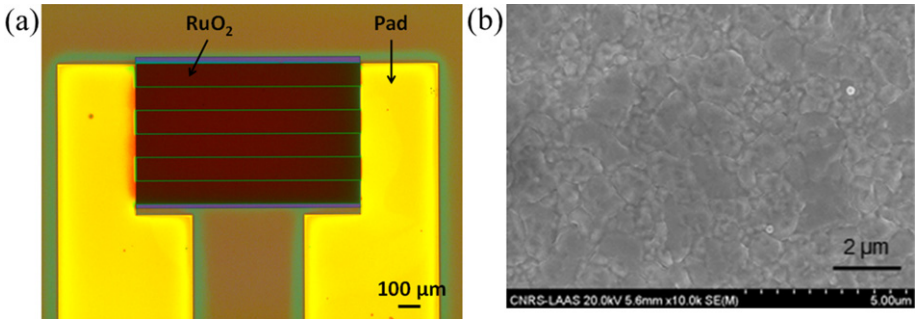

Fig. 4. (a) Optical image of the interdigital fingers after RuO_2 electrodeposition, and (b) SEM image of RuO_2 deposits.

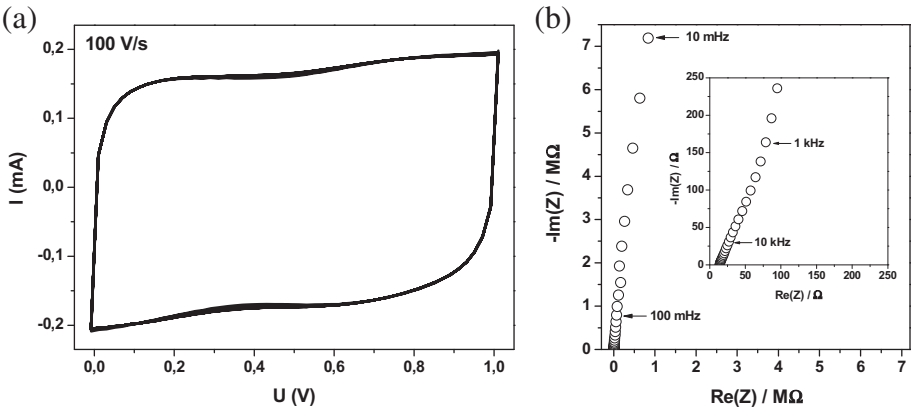

Fig. 5. (a) CVs at 100 V s^{-1} and (b) EIS of a $i = 5$ µm, $w = 1000$ µm, $L = 1000$ µm and $N = 6$ RuO_2 µ-SC.

of interdigitated fingers, Fig. 3(d) shows that E_{fp} is independent of N with a constant ratio $(A_a/A_{fp}) = (w \times L)/(1700 \times (w + i)) = 56\%$. However, the variation of P_{fp} shows an optimum for $N = 6$. This is related to the fact that $(R_{cc} \cdot A_{fp})$ increases and $(R_e \cdot A_{fp})$ decreases with increasing N values.

Accordingly, the following configuration was chosen as a compromise between high specific energy and high specific power: $i = 5$ µm, $L = 1000$ µm, $w = 100$ µm and $N = 6$.

3.3.2. *Validation with RuO_2 based micro-supercapacitors*

The electrodeposition of hydrous RuO_2 was performed on interdigitated gold electrodes. The adherence of the deposit was good and no short-circuit was observed for the 5 µm interspace (Fig. 4).

The RuO_2 µ-SC with the $i = 5$ µm – $L = 1000$ µm – $w = 100$ µm – $N = 6$ configuration maintains a stable capacitive behavior up to 100 V s^{-1} (Fig. 5(a)) with a cell capacitance of 0.2 mF cm^{-2} per footprint area ($A_{fp} = 1.1$ mm^2). The corresponding specific energy E_{fp} at 100 V s^{-1} is 84 µJ cm^{-2}. This result is comparable to our previous results obtained with onion-like carbon [15]. This ability to cycle at such high scan rates is due to the low value of the *RC* time constant of the interdigitated micro-supercapacitors (25 µs), *i.e.* a low absolute capacitance C and a low cell resistance R [27].

Fig. 5(b) displays the experimental Nyquist plot of the micro-device in deaerated 0.5 M H_2SO_4 electrolyte. No leakage current is observed, with a near vertical straight line in the low-frequency region typical of capacitive material. As expected, the value of the EDR of the RuO_2 thin film is very small (EDR < 1 Ω) and negligible compared to the value of the ESR (*ca.* 14 Ω), which is close to the predicted value (Fig. 2(d)). The corresponding specific power P_{fp} for this configuration is very high, with a value of 1.7 W cm^{-2}, in agreement with the proposed model (2.3 W cm^{-2}, Fig. 3(d)).

4. Conclusions

Based on a simple model, calculations were performed and compared with experimental data to find the electrode's optimal configuration of interdigitated RuO_2 based micro-supercapacitors. It was shown that an appropriate geometric adjustment of the electrode patterning can enhance the specific energy and specific power of the micro-devices, especially with the reduction of the physical separation isolating the interdigitated fingers. Electrodeposition of hydrous RuO_2 is a promising way to obtain high resolution micro-supercapacitors with interspace as low as 5 µm, and micro-devices able to cycle at a scan rate of 100 V s^{-1}. The use of conventional UV-photolithography techniques (1 µm resolution) currently limits the size of the pattern, but further work will consider the use of the stepper projection lithography (350 nm resolution), electron beam lithography or nanoimprint lithography (sub-10 nm resolution) for further reduction of the interspace. In turn, these improvements should lead to further increase of the specific power. Also, an optimization of the electrodeposition process of the RuO_2 should easily allow increasing the cell capacitance without any loss in the resolution of the device [28].

Acknowledgments

This work was partly supported by the French RENATECH network and financially supported by the French National Research Agency (ANR) through the MIDISTOCK project. T.M. Dinh was supported by a PhD grant and a travel fellowship (ATUPS) from the Université de Toulouse. Collaborations between LAAS and INRS were supported by the Commission Permanente de Coopération Franco-Québécoise (CPCFQ). One of us (D. Guay) would also like to acknowledge the Canada Research Chair program for its financial support.

References

[1] Z.L. Wang, Adv. Mater. 24 (2012) 280–285.
[2] R. Salot, S. Martin, S. Oukassi, M. Bedjaoui, J. Ubrig, Appl. Surf. Sci. 256 (2009) 54–57.
[3] Y.S. Yoon, W.I. Cho, J.H. Lim, D.J. Choi, J. Power Sources 101 (2001) 126–129.
[4] J.H. Lim, D.J. Choi, H.-K. Kim, W.I. Cho, Y.S. Yoon, J. Electrochem. Soc. 148 (2001) A275–A278.
[5] H.-K. Kim, S.-H. Cho, Y.-W. Ok, T.-Y. Seong, Y.S. Yoon, J. Vac. Sci. Technol. B 21 (2003) 949–952.
[6] M.-J. Lee, J.S. Kim, S.H. Choi, J.J. Lee, S.H. Kim, S.H. Jee, Y.S. Yoon, J. Electroceram. 17 (2006) 639–643.
[7] C.C. Ho, D.A. Steingart, J.P. Salminen, W.H. Sin, T.M.K. Rantala, J.W. Ewans, P.K. Wright, PowerMEMS, Berkeley, USA, November 29th–December 1st 2006.
[8] F.E. Kamel, P. Gonon, J. Vac. Sci. Technol. A 30 (2012). 04D1101–04D1106.
[9] J.-H. Sung, S.-J. Kim, K.-H. Lee, J. Power Sources 124 (2003) 343–350.
[10] J.-H. Sung, S.-J. Kim, K.-H. Lee, J. Power Sources 133 (2004) 312–319.
[11] J.-H. Sung, S.-J. Kim, S.-H. Jeong, E.-H. Kim, K.-H. Lee, J. Power Sources 162 (2006) 1467–1470.
[12] W. Sun, R. Zheng, X. Chen, J. Power Sources 195 (2010) 7120–7125.
[13] M. Beidaghi, C. Wang, Electrochim. Acta 56 (2011) 9508–9514.
[14] D. Pech, M. Brunet, P.-L. Taberna, P. Simon, N. Fabre, F. Mesnilgrente, V. Conédéra, H. Durou, J. Power Sources 195 (2010) 1266–1269.
[15] D. Pech, M. Brunet, H. Durou, P. Huang, V. Mochalin, Y. Gogotsi, P.-L. Taberna, P. Simon, Nat. Nanotechnol. 5 (2010) 651–654.
[16] H. Durou, D. Pech, D. Colin, P. Simon, P.-L. Taberna, M. Brunet, Microsyst. Technol. 18 (2012) 467–473.
[17] P. Huang, M. Heon, D. Pech, M. Brunet, P.-L. Taberna, Y. Gogotsi, S. Lofland, J.D. Hettinger, P. Simon, J. Power Sources 225 (2013) 240–244.
[18] W. Gao, N. Singh, L. Song, Z. Liu, A.L.M. Reddy, L. Ci, R. Vajtai, Q. Zhang, B. Wei, P.M. Ajayan, Nat. Nanotechnol. 6 (2011) 496–500.
[19] C. Shen, X. Wang, W. Zhang, F. Kang, J. Power Sources 196 (2011) 10465–10471.
[20] V. Zadin, D. Brandell, H. Kasemägi, A. Aabloo, J.O. Thomas, Solid State Ionics 192 (2011) 279–283.
[21] C.-C. Liu, D.-S. Tsai, D. Susanti, W.-C. Yeh, Y.-S. Huang, F.-J. Liu, Electrochim. Acta 55 (2010) 5768–5774.
[22] C.-C. Hu, Y.-H. Huang, J. Electrochem. Soc. 146 (1999) 2465–2471.
[23] R. Kötz, M. Carlen, Electrochim. Acta 45 (2000) 2483–2498.
[24] J.R. Miller, R.A. Outlaw, B.C. Holloway, Science 329 (2010) 1637–1639.
[25] K. Sheng, Y. Sun, C. Li, W. Yuan, G. Shi, Sci. Rep. 2 (2012) 1–5.
[26] W. Olthuis, W. Streekstra, P. Bergveld, Sens. Actuator B 24-25 (1995) 252–256.
[27] W.G. Pell, B.E. Conway, J. Power Sources 96 (2001) 57–67.
[28] K. Armstrong, T.M. Dinh, D. Pech, M. Brunet, J. Gaudet, D. Guay, MRS Fall Meeting, Boston, USA, November 25–30, 2012.